Review

Magnetic Nanoparticles in the Imaging of Tumor Angiogenesis

Shaunagh McDermott [1,*] and Alexander R. Guimaraes [1,2]

[1] Abdominal Imaging & Interventional Radiology, Massachusetts General Hospital, 55 Fruit St, Boston, MA 02114, USA

[2] Athinoula A. Martinos Center for Biomedical Imaging, 149 Thirteenth St, Suite 2301, Charlestown, MA 02129, USA; E-Mail: aguimaraes@mgh.harvard.edu

* Author to whom correspondence should be addressed; E-Mail: smcdermott1@partners.org; Tel.: +1-617-726-8396; Fax: +1-617-726-4891.

Abstract: Angiogenesis, the growth of new capillary blood vessels, is central to the growth of tumors. Non-invasive imaging of tumor angiogenesis will allow for earlier detection of tumors and also the development of surrogate markers for assessing response to treatment. Steady state magnetic resonance imaging with magnetic nanoparticles is one method to assess angiogenesis. In this article we explain the theory behind steady state magnetic resonance imaging and review the available literature.

Keywords: angiogenesis; ultrasmall superparamagnetic iron oxide; magnetic resonance imaging

1. Introduction

Tumor growth and metastasis formation are dependent on angiogenesis, the process of new blood vessel formation [1]. Typically tumor-associated angiogenesis goes through two phases, an avascular and a vascular phase that are separated by the "angiogenic switch". The avascular phase of tumors corresponds to small occult lesions that stay dormant and subside on diffusion of nutrients from the host microvasculature. After reaching a certain size (usually around 1–2 mm), a small subset of dormant tumors enter the vascular phase in which exponential tumor growth ensues. Angiogenesis is a complex multistep process regulated by many factors. At the onset of angiogenesis, a number of pro-angiogenic growth factors (e.g., vascular endothelial growth factors, platelet derived growth factor, fibroblast growth factors) and proteolytic enzymes (e.g., metalloproteinases, cathepsin cysteine

proteases, plasmin) are secreted into the interstitium. This leads to degradation of basal membrane surrounding the pre-existing vasculature, along with proliferation and migration of smooth muscle and endothelial cells. All these events lead to the alignment and organization of endothelial cells to form new vessels and a vascular network within the tumor [2–4].

Tumor angiogenesis is not simply the production of an increased number of blood vessels to serve a growing tumor mass. Although the main purpose of tumor angiogenesis can be considered to maintain a cancer's blood supply, the process occurs in an unmitigated fashion, and the resultant vascular network is highly abnormal [1]. This profoundly aberrant vasculature dramatically alters the tumor microenvironment and influences heavily the ways in which cancers grow and progress, escape the host's immune system, metastasize, and respond to anticancer therapies [5].
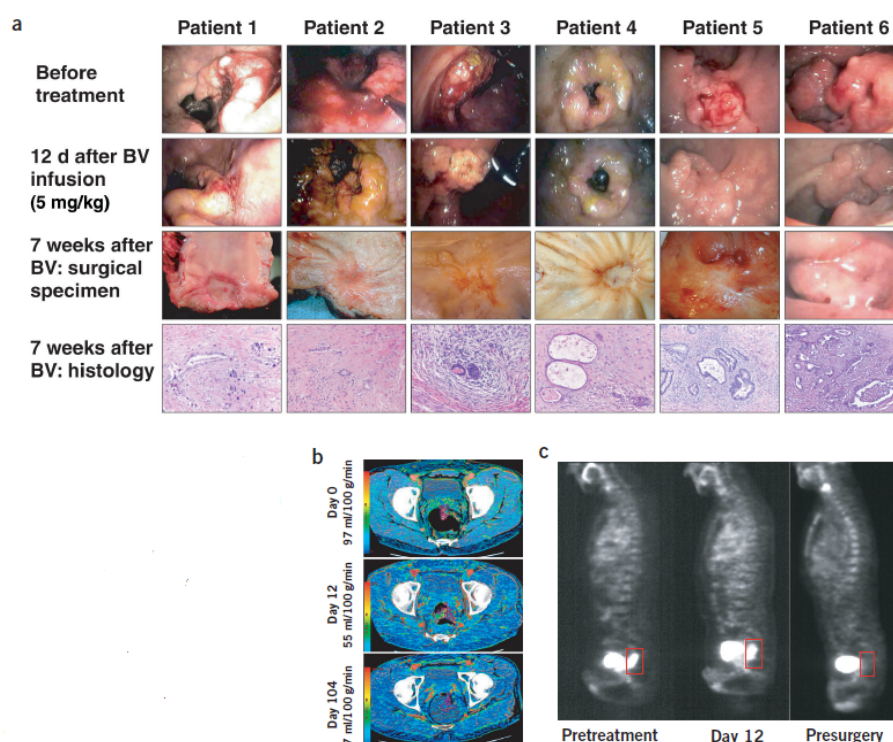
The heterogeneity in vessel distribution and haphazard anatomical arrangement of the vasculature cause spatial and temporal heterogeneity in blood flow, with areas of hypervasularity adjacent to hypovascular ones [6]. Also, the structural abnormalities of the tumor vasculature lead to a marked increase in vessel leakiness. As a consequence, there is a protein and fluid build-up in the tumor interstitium. This excess extravasation of protein increases the extravascular oncotic pressure, dragging further fluid into the interstitial space [6,7]. Furthermore, there is an absence of functional intratumoral lymphatic vessels, resulting in the impaired clearance of extracellular fluid and hence interstitial hypertension within tumors. The raised intratumoral interstitial fluid pressure (IFP) reduces the hydrostatic pressure gradient between the intravascular and extravascular compartments such that the two essentially equilibrate, which reduces transvascular flow. Moreover, the mechanical stress from the solid mass of proliferating cancer cells and the matrix is able to collapse tumor vessels, closing the lumen through compressive forces [8]. This combination of regional poor perfusion, raised IFP, and areas of vascular collapse produces regional hypoxia and acidosis within tumors [9], with major implications for tumor sensitivity to therapy. Hypoxia is a well-known mediator of cancer cell resistance to conventional radiotherapy and cytotoxics [10,11]. Moreover, the poor blood supply and raised intratumoral IFP (leading to a reduction in transvascular flow) impair the delivery of systemically administered therapies, such as conventional cytotoxics and monoclonal antibodies, to tumors [6,12].

With the discovery of vascular endothelial growth factor (VEGF) as a major driver of tumor angiogenesis, efforts were focused on novel therapeutics aimed at inhibiting VEGF activity, with the goal of regressing tumors by starvation. Unfortunately, clinical trials of anti-VEGF monotherapy in patients with solid tumors have been largely negative [13]. Intriguingly, the combination of anti-VEGF therapy with conventional chemotherapy has improved survival in cancer patients compared with chemotherapy alone [14,15]. In 2001, a "vascular normalization" hypothesis was proposed to explain this paradox [16]. The normalization hypothesis suggests that by correcting the abnormalities in structure and function of tumor vessels (rather than destroying vessels completely) a normalization of the tumor microenvironment and ultimately control tumor progression can be achieved due to improved response to intravenous as well as radiation therapy [5].

In clinical practice, angiogenesis is assessed in terms of microvessel density as determined on surgical biopsy specimens [17]. Whereas biopsies provide information only from particular regions within the tumor, the vasculature of high-grade tumors is highly heterogeneous [4]. Necrotic areas exhibit sparse and degraded vessels, whereas angiogenic areas are characterized by high vessel density [18], large vessel diameters [19], and increased permeability. *In vivo* imaging methods for

monitoring microvasculature non-invasively are therefore of major interest for both tumor detection and the development of surrogate markers for assessing response to treatment (Figure 1).

> **Figure 1.** Effect of treatment on tumors in patients who completed entire combined treatment regimen, and surgery. (**a**) Endoscopic and pathological evaluation of rectal tumors. Surgical specimens showed grade II tumor regression in patients 1–5 and grade III in patients 6, by Mandard criteria. Endoscopic image (instead of surgical specimen) was taken for patients 6, 3.5 weeks before surgery. BV, bevacizumab. (**b**) Representative functional CT images of blood perfusion before treatment (day 0), after bevacizumab (day 12) and after completion of treatment (day 104) in patient 5. (**c**) Tumor FDG uptake before treatment (pretreatment), 12d after bevacizumab treatment and 6–7 weeks after completion of all neoadjuvant therapy (presurgery). Saggital projections of FDG-PET scans for patient 1 are shown. Tumor is outlined in box, posterior to the bladder. Reprinted with permission from Macmillan Publishers Ltd: Nature Medicine, Willet *et al.* Direct evidence that the VEGF-specific antibody bevacizumab has antivascular effects in human rectal cancer. 2004, *10*, 145–147.

Imaging angiogenesis has been focused into three different arenas: (1) steady state blood volume determinations of neovascular density using magnetic nanoparticles; (2) kinetic imaging using dynamic tracking of contrast administration by ultrasound, computed tomography or magnetic resonance imaging; and (3) specific molecular markers of angiogenesis. This article will focus on steady state imaging of angiogenesis using magnetic nanoparticles, which as described below, does not suffer from some of the pitfalls associated with kinetic techniques (*i.e.*, two *vs.* three compartment modeling, tradeoffs between spatial and temporal resolution, ability to image in areas constrained by motion), and offers high spatial resolution imaging of the blood pool with sophisticated analyses of microvascular volume and vessel size.

2. Steady State Imaging Using Magnetic Nanoparticles

Ultrasmall super paramagnetic iron oxide (USPIO) (a.k.a. magnetic nanoparticle (MNP)) is a steady state blood pool agent that creates contrast in magnetic resonance imaging (MRI) through magnetic susceptibility variations proximal to the vascular network [20–23], which results in changes in inherent and induced transverse relaxation times defined as T_2 and T_2^*, respectively. Accurate evaluation of $R_2^*(1/T_2^*)$ or $R_2(1/T_2)$ necessitate defining two or more points on the natural or induced transverse relaxation decay curve. Addition of contrast agent increases $R_2^*(1/T_2^*)$ thus causing limits on sampling as the T_2^* is shortened. It can be shown that:

$$\Delta R_2^* \text{ or } \Delta R_2 \propto \log [S^{post}/S^{pre}]$$

where, S^{pre} ad S^{post} are pre- and post-contrast MRI signal intensity [24]. A fundamental assumption is that the change in the transverse relaxation rate ($[\Delta R_2 = 1/\Delta T_2]$ and $[\Delta R_2^* = 1/\Delta T_2^*]$) relative to the preinjection baseline is proportional to the perfused local blood volume per unit tumor volume (V) multiplied by a function (f) of the plasma concentration of the agent (P) [25–27].

$$\Delta R_2 = kf(P) \cdot V$$

Therefore, the capability of MNP to modulate the effective transverse relaxation rate, R_2^*, is exploited where the difference image of R_2^* before and after administration of MNP will be useful in determining microvessel density [28].

A gradient echo (GE) MRI sequence allows blood volume (BV) assessment in relatively shorter data acquisition times and has the advantage of minimizing artifacts associated with flow effects. A recent report with a brain tumor model also showed that the R_2^* is more sensitive to the MNP induced susceptibility change [29] and can be used to estimate tumor BV. Although BV is linearly proportional to ΔR_2 and ΔR_2^*, the proportionality constant was shown to be contrast agent dose-dependent [30]. The apparent BV values of tissues with different composition of arteries, capillaries, and veins were shown to be different [30] since ΔR_2 and ΔR_2^* are affected by vessel size [31]. The ΔR_2 peaks for vessels 1–2 μm in diameter whereas ΔR_2^* is fairly independent of vessel size beyond 3–4 μm. These studies thus provide the rationale for spin-echo imaging being more sensitive to microvasculature, while gradient-echo imaging is more sensitive to total vasculature.

3. Translational Studies

For magnetic nanoparticles to be useful in the assessment of tumor angiogenesis, it is important that the particles stay within the intravascular system, can characterize with tumor microvasculature and can monitor response to antiangiogenic therapy. Furthermore, can targeted nanoparticles be synthesized that target specific markers of angiogenesis.

3.1. Are Magnetic Nanoparticles Truly Intravascular Agents?

Bremer *et al.* first utilized intravital microscopy to determine whether a prototype magnetic nanoparticle agent (MION) truly had intravascular distribution in tumor microenvironment [25]. For these experiments a green fluorescent protein expressing 9 L tumor model was utilized, in which tumor microvasculature is clearly outlined against fluorescent tumor cells, even at very high spatial
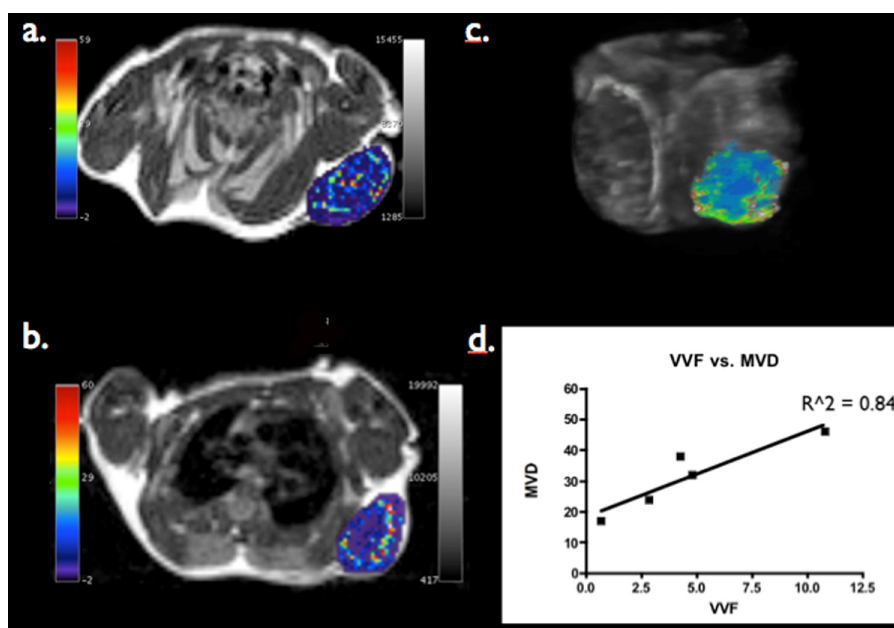
resolution, which demonstrated that MION selectively enhanced the vascularity without any significant leakage into tumor interstitium during time of observation (30 min). They also found that steady state measures of vascular volume fraction (VVF) with MRI allow for volumetric, *in vivo*, non-invasive assay of microvascular density in experimental tumor models.

Another study by Lemasson assessed whether USPIO extravasated in their tumor model within the time frame of the MR session [32]. They found that the extravascular concentration of USPIO in the tumor was, at most, 0.3% of the plasma concentration twenty minutes after injection. This result validated the main hypothesis of vessel size index (VSI) and BVf (blood volume fraction) measurement: that USPIO remains as an intravascular contrast agent.

3.2. Can Steady State MRI Characterize Tumor Microvasculature?

A study was performed by Valable *et al.* [33] found a significant correlation between BVf_{MRI} and BVf_{histo} ($P < 0.005$) and VSI_{MRI} and VSI_{histo} ($P < 0.0001$) in two rat models of glioma, however MRI provided estimates that are larger by a factor of ~2. Another study by Beaumont *et al.* [34], also found that the blood volume fraction estimates (steady-state MRI approach) were larger than histologic estimates (BVf_{histo}). Studies by Guimeraes *et al.* on nude mice implanted with renal cell [35] and pancreatic cancer [36] (Figure 2), found excellent correlation between VVF and MVD ($R^2 = 0.95$ and 0.85, respectively).
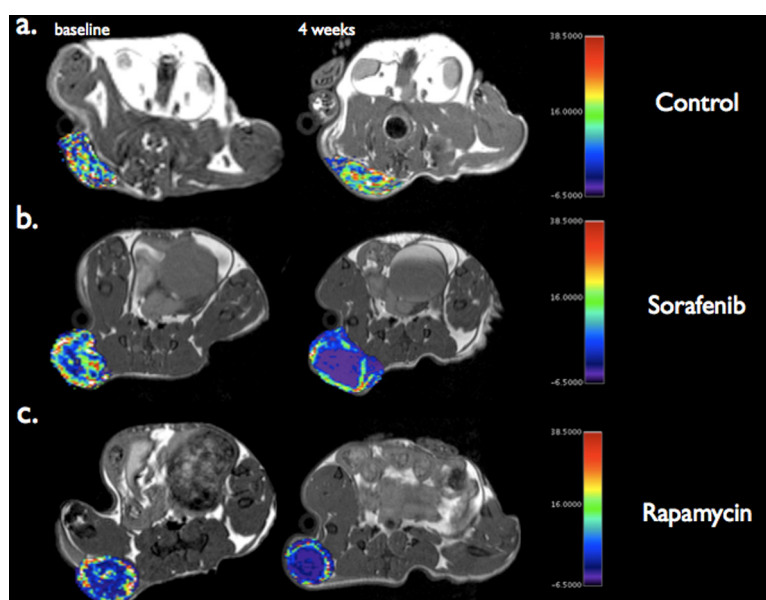
Figure 2. T1-weighted MRI of mice with pseudocolorized VVF maps superimposed over the center of the tumor within the left flank prior to (**a**) and following (**b**) the administration of ShH antibody. Note the heterogeneity of signal intensity and color spread at baseline, with marked decrease in vascularity in the post-treated mouse as compared to pre-baseline. (**c**) 3dimensional VVF map of the mouse tumor in the left flank. (**d**) VVF was quantified in all treated mice and correlated histologically to anti-CD-31 microvessel density. Note the excellent correlation of VVF to MVD. Figure from Guimaraes *et al.* (unpublished data).

3.3. Can Steady State MRI Monitor Response to Anti-Angiogenic Therapy?

Guimeraes *et al.* [35] also studied the effect of anti-angiogenic therapies (rapamycin (mTOR inhibitor) and sorafenib (VEGF inhibitor) on renal cell carcinoma using MRI with magnetic nanoparticles. They found that the VVF in all treatment arms differed from control (P < 0.05) and declined weekly with treatment (Figure 3).

Figure 3. T1-weighted MRI of mice with pseudocolorized VVF maps superimposed over the center of the tumor within the right flank for each treatment arm (control (**a**), sorafenib (**b**), and Rapamycin (**c**)) of the trial at baseline, and at the end of therapy. Note the heterogeneity of signal intensity and color spread throughout all cohorts at baseline, with marked decrease in vascularity in the rapamycin (b) and sorafenib (c) treated animals as compared to control (a). Of note, only 3 mice survived all 3 weeks of therapy within the rapamycin treated arm. Figure from Guimaraes *et al*. (unpublished data)

Persigehl *et al.* [22] investigated steady state blood volume measurements for early quantitative monitoring of anti-angiogenic treatment of fibrosarcoma bearing nude mice. They found that the VVF measured with USPIO-enhanced MR imaging correlated well with the grade of tumor thrombosis, necrosis or both. Moreover, the MR data were in line with independent perfusion measurements obtained by using fluorescent intravascular microspheres. A second study by the same group found that for responders there was a significant decrease in ΔR_2^* and VVF compared with the control group, whereas ΔR_2^* and VVF remained nearly unchanged for nonresponders [37].

Another study by Guimaraes *et al.* [36] tested whether MR imaging measures of VVF using magnetic iron oxide nanoparticles were sensitive to the anti-angiogenic effect of targeted sonic hedgehog (Shh) therapies in a pancreatic cancer xenograft model. They found that in response to anti-Hh treatment, tumors showed a decrease in VVF compared with controls (P < 0.001).

Lemasson *et al.* [32] performed a study on nude mice implanted with human glioma cells comparing cytotoxic and anti-angiogenic drug effects using multiparametric MRI. In mice treated with an anti-angiogenic therapy (Sorafenib), the tumoral VSI was significantly larger than in the untreated

group. Also in the Sorafenib group, tumoral BVf decreased from treatment onset, whereas it remained stable in the untreated groups. VSI and BVf in the cytotoxic group did not differ from the values measured in the untreated group.

A study by Hyodo *et al.* [28] to evaluate the anti-angiogenic effect of Sunitinib in squamous cell carcinoma tumor bearing mice revealed ~46% reduction in tumor blood volume 4 days after start of Sunitinib treatment.

Ring *et al.* evaluated whether "steady state" MRI using a robust multiecho ΔR_2^* MR relaxometry technique was suitable for the early assessment of rahbdomyosarcoma-bearing mice treated with bevacizumab [38]. They found that the bevacizumab resulted in a significant reduction of the ΔR_2^* values compared with the control group, reflecting a significant decrease of the VVF by 33%. Immunohistochemistry confirmed the MR results showing an approximately 25% reduction of the MVD after treatment.

3.4. Can targeted Nanoparticles Bind to Markers of Angiogenesis?

A study using arginine-glycine-aspartic acid (RGD) nanoparticles targeting integrins on BT-20 tumor found three factors associated with the ability of nanoparticles to target tumor cell integrins— tumor cell integrin expression; nanoparticle pharmacokinetics; and tumor vascularization [39]. Zhang *et al.* conjugated the RGD peptide, which binds to the $\alpha_v\beta_3$integrin receptor, to 3-aminopropyltrimethoxysilane-coated magnetic nanoparticles and administered them to nude mice bearing tumors with different levels of $\alpha_v\beta_3$ integrin-positive vessels. Results showed that RGD nanoparticles targeted to the tumor vessels and the change in T2 relaxation was related to the degree of expression of $\alpha_v\beta_3$integrin detected by 1.5T MR scanner [40]. A further study on melanoma-bearing mice, found that the percentage of MR signal-enhanced voxels was low and increased in animal receiving $\alpha_v\beta_3$- and Robo4-targeted nanoparticles [41]. The same group demonstrated the use of a new paramagnetic nanoparticle formulation targeted to $\alpha_5\beta_1$-integrin positive neovasculature for both delivering anti-angiogenic therapy and detecting the tumor response [42].

4. Conclusions

Angiogenesis is an essential factor of tumor blood supply and consequently disease progression. Assessing angiogenesis is important when determining tumor grade and prognosis. Anti-angiogenic treatment is an emerging strategy not only to suppress the tumor growth by shutting off the nutrient and oxygen supply to tumors but also to improve the efficiency of cytotoxic drugs and radiotherapy via transit vascular normalization. Imaging has an important role in identifying patients who are likely to benefit from these new anti-angiogenic treatments and also to assess response to treatment.

References

1. Folkman, J. Angiogenesis research: From laboratory to clinic. *Forum (Genova)* **1999**, *9*, 59–62.
2. Bergers, G.; Benjamin, L.E. Tumorigenesis and the angiogenic switch. *Nat. Rev. Cancer.* **2003**, *3*, 401–410.
3. Hanahan, D.; Folkman, J. Patterns and emerging mechanisms of the angiogenic switch during tumorigenesis. *Cell* **1996**, 86, 353–364.

4. Folkman, J. Role of angiogenesis in tumor growth and metastasis. *Semin Oncol.* **2002**, *29*, 15–18.

5. Jain, R.K. Normalization of tumor vasculature: An emerging concept in antiangiogenic therapy. *Science* **2005**, 307, 58–62.

6. Tong, R.T.; Boucher, Y.; Kozin, S.V.; Winkler, F.; Hicklin, D.J.; Jain, R.K. Vascular normalization by vascular endothelial growth factor receptor 2 blockade induces a pressure gradient across the vasculature and improves drug penetration in tumors. *Cancer Res.* **2004**, *64*, 3731–3736.

7. Stohrer, M.; Boucher, Y.; Stangassinger, M.; Jain, R.K. Oncotic pressure in solid tumors is elevated. *Cancer Res.* **2000**, *60*, 4251–4255.

8. Padera, T.P.; Stoll, B.R.; Tooredman, J.B.; Capen, D.; di Tomaso, E.; Jain, R.K. Pathology: Cancer cells compress intratumour vessels. *Nature* **2004**, *427*, 695.

9. Helmlinger, G.; Yuan, F.; Dellian, M.; Jain, R.K. Interstitial pH and pO_2 gradients in solid tumors *in vivo*: High-resolution measurements reveal a lack of correlation. *Nat. Med.* **1997**, *3*, 177–182.

10. Teicher, B.A. A systems approach to cancer therapy. (Antioncogenics + standard cytotoxics → mechanism(s) of interaction). *Cancer Metastasis Rev.* **1996**, *15*, 247–272.

11. Wouters, B.G.; Brown, J.M. Cells at intermediate oxygen levels can be more important than the "hypoxic fraction" in determining tumor response to fractionated radiotherapy. *Radiat Res.* **1997**, *147*, 541–550.

12. Jain, R.K. Delivery of novel therapeutic agents in tumors: physiological barriers and strategies. *J Natl. Cancer Inst.* **1989**, *81*, 570–576.

13. Jain, R.K.; Duda, D.G.; Clark, J.W.; Loeffler, J.S. Lessons from phase III clinical trials on anti-VEGF therapy for cancer. *Nat. Clin. Pract. Oncol.* **2006**, *3*, 24–40.

14. Sandler, A.; Gray, R.; Perry, M.C.; Brahmer, J.; Schiller, J.H.; Dowlati, A.; Lilenbaum, R.; Johnson, D.H. Paclitaxel-carboplatin alone or with bevacizumab for non-small-cell lung cancer. *N. Engl. J. Med.* **2006**, *355*, 2542–2550.

15. Saltz, L.B.; Clarke, S.; Diaz-Rubio, E.; Scheithauer, W.; Figer, A.; Wong, R.; Koski, S.; Lichinitser, M.; Yang, T.S.; Rivera, F.; *et al*. Bevacizumab in combination with oxaliplatin-based chemotherapy as first-line therapy in metastatic colorectal cancer: a randomized phase III study. *J. Clin. Oncol.* **2008**, 2*6*, 2013–2019.

16. Jain, R.K. Normalizing tumor vasculature with anti-angiogenic therapy: A new paradigm for combination therapy. *Nat. Med.* **2001**, *7*, 987–989.

17. Takei, H.; Bhattacharjee, M.B.; Rivera, A.; Dancer, Y.; Powell, S.Z. New immunohistochemical markers in the evaluation of central nervous system tumors: A review of 7 selected adult and pediatric brain tumors. *Arch. Pathol. Lab. Med.* **2007**, *131*, 234–241.

18. Carmeliet, P.; Jain, R.K. Angiogenesis in cancer and other diseases. *Nature* **2000**, 407, 249–257.

19. Brown, E.B.; Campbell, R.B.; Tsuzuki, Y.; Xu, L.; Carmeliet, P.; Fukumura, D.; Jain, R.K. *In vivo* measurement of gene expression, angiogenesis and physiological function in tumors using multiphoton laser scanning microscopy. *Nat. Med.* **2001**, *7*, 864–868.

20. Corot, C.; Robert, P.; Idee, J.M.; Port, M. Recent advances in iron oxide nanocrystal technology for medical imaging. *Adv. Drug Deliv. Rev.* **2006**, *58*, 1471–1504.

21. Enochs, W.S.; Harsh, G.; Hochberg, F.; Weissleder, R. Improved delineation of human brain tumors on MR images using a long-circulating, superparamagnetic iron oxide agent. *J. Magn. Reson. Imaging*. **1999**, *9*, 228–232.

22. Persigehl, T.; Bieker, R.; Matuszewski, L.; Wall, A.; Kessler, T.; Kooijman, H.; Meier, N.; Ebert, W.; Berdel, W.E.; Heindel, W.; *et al*. Antiangiogenic tumor treatment: early noninvasive monitoring with USPIO-enhanced MR imaging in mice. *Radiology* **2007**, *244*, 449–456.

23. Tropres, I.; Grimault, S.; Vaeth, A.; Grillon, E.; Julien, C.; Payen, J.F.; Lamalle, L.; Decorps, M. Vessel size imaging. *Magn. Reson. Med*. **2001**, *45*, 397–408.

24. Brown, J.M.; Giaccia, A.J. The unique physiology of solid tumors: opportunities (and problems) for cancer therapy. *Cancer Res*. **1998**, *58*, 1408–1416.

25. Bremer, C.; Mustafa, M.; Bogdanov, A., Jr., Ntziachristos, V.; Petrovsky, A.; Weissleder, R. Steady-state blood volume measurements in experimental tumors with different angiogenic burdens a study in mice. *Radiology* **2003**, *226*, 214–220.

26. Boxerman, J.L.; Hamberg, L.M.; Rosen, B.R.; Weisskoff, R.M. MR contrast due to intravascular magnetic susceptibility perturbations. *Magn. Reson. Med*. **1995**, *34*, 555–566.

27. Dennie, J.; Mandeville, J.B.; Boxerman, J.L.; Packard, S.D.; Rosen, B.R.; Weisskoff, R.M. NMR imaging of changes in vascular morphology due to tumor angiogenesis. *Magn. Reson. Med.* **1998**, *40*, 793–799.

28. Hyodo, F.; Chandramouli, G.V.; Matsumoto, S.; Matsumoto, K.; Mitchell, J.B.; Krishna, M.C.; Munasinghe, J.P. Estimation of tumor microvessel density by MRI using a blood pool contrast agent. *Int. J. Oncol.* **2009**, *35*, 797–804.

29. Gambarota, G.; Leenders, W.; Maass, C.; Wesseling, P.; van der Kogel, B.; van Tellingen, O.; Heerschap, A. Characterisation of tumour vasculature in mouse brain by USPIO contrast-enhanced MRI. *Br. J. Cancer*. **2008**, *98*, 1784–1789.

30. Pathak, A.P.; Rand, S.D.; Schmainda, K.M. The effect of brain tumor angiogenesis on the *in vivo* relationship between the gradient-echo relaxation rate change (DeltaR2*) and contrast agent (MION) dose. *J. Magn. Reson. Imaging*. **2003**, *18*, 397–403.

31. Kiselev, V.G.; Strecker, R.; Ziyeh, S.; Speck, O.; Hennig, J. Vessel size imaging in humans. *Magn. Reson. Med*. **2005**, *53*, 553–563.

32. Lemasson, B.; Christen, T.; Tizon, X.; Farion, R.; Fondraz, N.; Provent, P.; Segebarth, C.; Barbier, E.L.; Genne, P.; Duchamp, O.; *et al*. Assessment of multiparametric MRI in a human glioma model to monitor cytotoxic and anti-angiogenic drug effects. *NMR Biomed*. **2011**, *24*, 473–482.

33. Valable, S.; Lemasson, B.; Farion, R.; Beaumont, M.; Segebarth, C.; Remy, C.; Barbier, E.L. Assessment of blood volume, vessel size, and the expression of angiogenic factors in two rat glioma models: A longitudinal *in vivo* and *ex vivo* study. *NMR Biomed*. **2008**, *21*, 1043–1056.

34. Beaumont, M.; Lemasson, B.; Farion, R.; Segebarth, C.; Remy, C.; Barbier, E.L. Characterization of tumor angiogenesis in rat brain using iron-based vessel size index MRI in combination with gadolinium-based dynamic contrast-enhanced MRI. *J. Cereb. Blood Flow Metab*. **2009**, *29*, 1714–1726.

35. Guimaraes, A.R.; Ross, R.; Figuereido, J.L.; Waterman, P.; Weissleder, R. MRI with magnetic nanoparticles monitors downstream anti-angiogenic effects of mTOR inhibition. *Mol. Imaging Biol.* **2011**, *13*, 314–320.

36. Guimaraes, A.R.; Rakhlin, E.; Weissleder, R.; Thayer, S.P. Magnetic resonance imaging monitors physiological changes with antihedgehog therapy in pancreatic adenocarcinoma xenograft model. *Pancreas* **2008**, *37*, 440–444.

37. Persigehl, T.; Matuszewski, L.; Kessler, T.; Wall, A.; Meier, N.; Ebert, W.; Berdel, W.E.; Heindel, W.; Mesters, R.; Bremer, C. Prediction of antiangiogenic treatment efficacy by iron oxide enhanced parametric magnetic resonance imaging. *Invest. Radiol.* **2007**, *42*, 791–796.

38. Ring, J.; Persigehl, T.; Remmele, S.; Heindel, W.; Dahnke, H.; Bremer, C. Monitoring of bevacizumab-induced antiangiogenic treatment effects by "steady state" ultrasmall superparamagnetic iron oxide particles magnetic resonance imaging using robust multiecho DeltaR2* relaxometry. *Invest Radiol.* **2011**, *46*, 326–330.

39. Montet, X.; Montet-Abou, K.; Reynolds, F.; Weissleder, R.; Josephson, L. Nanoparticle imaging of integrins on tumor cells. *Neoplasia* **2006**, *8*, 214–222.

40. Zhang, C.; Jugold, M.; Woenne, E.C.; Lammers, T.; Morgenstern, B.; Mueller, M.M.; Zentgraf, H.; Bock, M.; Eisenhut, M.; Semmler, W.; *et al*. Specific targeting of tumor angiogenesis by RGD-conjugated ultrasmall superparamagnetic iron oxide particles using a clinical 1.5-T magnetic resonance scanner. *Cancer Res.* **2007**, *67*, 1555–1562.

41. Boles, K.S.; Schmieder, A.H.; Koch, A.W.; Carano, R.A.; Wu, Y.; Caruthers, S.D.; Tong, R.K.; Stawicki, S.; Hu, G.; Scott, M.J.; *et al*. MR angiogenesis imaging with Robo4- *vs.* alphaVbeta3-targeted nanoparticles in a B16/F10 mouse melanoma model. *Faseb J.* **2010**, *24*, 4262–4270.

42. Schmieder, A.H.; Caruthers, S.D.; Zhang, H.; Williams, T.A.; Robertson, J.D.; Wickline, S.A.; Lanza, G.M. Three-dimensional MR mapping of angiogenesis with $\alpha_5\beta_1(\alpha_v\beta_3)$-targeted theranostic nanoparticles in the MDA-MB-435 xenograft mouse model. *Faseb J.* **2008**, 22, 4179–4189.